Malaysian Journal of Chemistry, 2016, Vol. 18(1), 9–26

Electrochemical Synthesis of a Metal Organic Framework Material Based on Copper and Benzene–1,3,5–Tricarboxylic Acid Using Applied Current

Thu Phuong Nguyen[1]*, Thi Nam Pham[1], Claudine Buess-Herman[2], Thi Thom Nguyen[1], Thi Mai Thanh Dinh[1]

[1] Institute for Tropical Technology, Vietnam Academy of Science and Technology, 18 Hoang Quoc Viet Street, Cau Giay district, Hanoi, Vietnam

[2] Chimie Analytique et Chimie des Interfaces, Faculté des Sciences, Université Libre de Bruxelles, Boulevard du Triomphe, 2, CP 255, B-1050 Bruxelles, Belgium

*Corresponding author (e-mail: ntphuong@itt.vast.vn)

Metal organic framework material based on copper and benzene–1,3,5–tricarboxylic acid (H3BTC) was synthesized by applying electric current method. The influences of applied current, $NaNO_3$ concentration, synthesis time and hydrate process to molecular and phase structure, morphology and specific surface area were studied. When the parameters of electrodeposition changed, CuBTC one dimension (1D) and three dimensions (3D) could be obtained. The optimum conditions to gain CuBTC 3D were: 100 mA current, $NaNO_3$ concentration of 0.05 M with synthesis time of 10 min. The short-time hydrate process could increase specific surface area from 79 m^2/g to 617 m^2/g, however, the long-time hydrate process could lead to the destruction of material structure.

Key words: Metal organic framework, CuBTC, electrodeposition, hydrate process

Received: November 2014; Accepted: March 2016

Metal organic framework (MOF) is a highly porous material group which is made of metallic ions (or clusters) co-ordinated to organic ligands to form 1-D, 2-D and 3-D structures with high adsorption ability and high specific surface area. MOF's flexibility gives rise to "breathing" phenomenon or gate-opening effect of its pores in response to external stimuli [1–4]. MOF was first synthesized by Prof Yaghi in 1995 [1]. In 1999, $Cu_3(BTC)_2$ (MOF-199 or HKUST) and MOF-5 were synthesized and they are two types of MOFs which were researched extensively [2]. There are many methods to synthesize MOF such as hydrothermal [3, 4], chemical [5], mechanochemical [6], microwave [7], sonochemical [8] and electrochemical [9–20]. The electrochemical synthesis has much potentials because it is capable of synthesizing large amount of pure material in a short time and the product mass can be controlled. MOF is widely applied in gas adsorption, gas separation [21], gas storage [1, 7, 22, 23], catalyst [11, 20, 24, 25], electrode, ionic exchange and medicine.

In the electrochemical method, we can use applied potential, applied current and scanning potential method to synthesize $Cu_3(BTC)_2$ based on copper and benzene–1,3,5–tricarboxylic acid. The morphology, structure and properties of MOF are affected by many factors in synthesis process such as organic ligand, metallic ions, solvents, conducting electrolyte, temperature, pH and synthesis method. Therefore, research to determine the optimum condition to synthesize MOF for application in different fields still attracts many scientists. This paper describes the investigation of influencing factors such as applied electric current, $NaNO_3$ electrolyte concentration, synthesis time and hydrate process to morphology and structure of MOF based on Cu and H3BTC.

EXPERIMENT METHOD

Chemical and Experiment

CuBTC was synthesized from benzene–1,3,5–tricarboxylic acid (H_3BTC, Merk; 95% purity, has formula $C_9H_6O_6$) and copper in methanol (CH_3OH, 99.5% purity) solutions of sodium nitrate ($NaNO_3$; 99% purity). CuBTC was synthesized in an electrochemical cell containing the solutions of various compositions as shown in Table 1.

We conducted the experiments to investigate the effect of following factors: applied current intensity (M1, M2, M3); the concentration of $NaNO_3$ conductor (M1, M4, M5); synthesis time (M1, M6, M7) and product hydrate process. The cell had three electrodes: saturated calomel electrode, working and counter electrodes were copper 99.61% and 20×50×3 mm in size. Copper electrodes were polished by polishing machine and 400, 800, 1200 SiC papers, rinsed in water and methanol. CuBTC synthesis experiments were conducted by Autolab equipment and Regulated Powersupply GP-1305TP by applied current method. The source of the metallic ion was the oxidation of the working copper electrode (anodic dissolution), and the released metallic ions reacted immediately with the organic linker present in the solution to form the MOF close to the electrode surface. MOF was not only formed as a dense film on copper but also as crystals in the solution. But we wanted to obtain a large amount of MOF powder for further application so that the powder could be analyzed. The powder was filtered, rinsed by methanol and dried at 60°C in oven for 15 h to conduct analytical studies.

Analysis Method

The characteristic groups of CuBTC were researched by FT-IR 6700 (Nicolet) in the range of wave numbers from 400–3000 cm^{-1}; the morphology was studied by SEM S4800 (Hitachi). The specific surface area of CuBTC was determined by BET method using a device Micromeritics TriStar 3000 V6.07A. From X-ray diffraction pattern (Siemens D5000 Bruker – Germany), the phase structure of CuBTC and the distance between lattice planes *d* could be determined. CuBTC 1D has monoclinic structure, CuBTC 3D has faced-centered cubic structure with a = b = c and $\alpha = \beta = \gamma = 90°$; from the Miller index (hkl) of CuBTC 3D, we could determine the lattice parameter using the following the equation:

$$d = \frac{a}{\sqrt{h^2 + k^2 + l^2}} \quad (*)$$

RESULTS AND DISCUSSIONS

The Effect of Applied Current Intensity

Figure 1 shows the variation of potential follow time of synthesis process of CuBTC at the different applied current intensity: 100 mA; 200 mA and 300 mA with the $NaNO_3$ 0.05 M conductor in 10 min. In general, the curves have the same shape, the first, responded to the potential increase faster due to the formation of double layers of BTC ions on the surface of the electrode; subsequently, the potentials obtained the stable value about 2, 4.3 and 6.1 V corresponding with CuBTC synthesis process at the applied current intensity of 100, 200 and 300 mA. The applied current intensity

Table 1. The component of the solutions to synthesize CuBTC in the different conditions.

Sample	[$NaNO_3$] (M)	Applied current intensity (mA)	Time (minutes)
M1	0.05	100	10
M2	0.05	200	10
M3	0.05	300	10
M4	0.1	100	10
M5	0.2	100	10
M6	0.05	100	20
M7	0.05	100	40

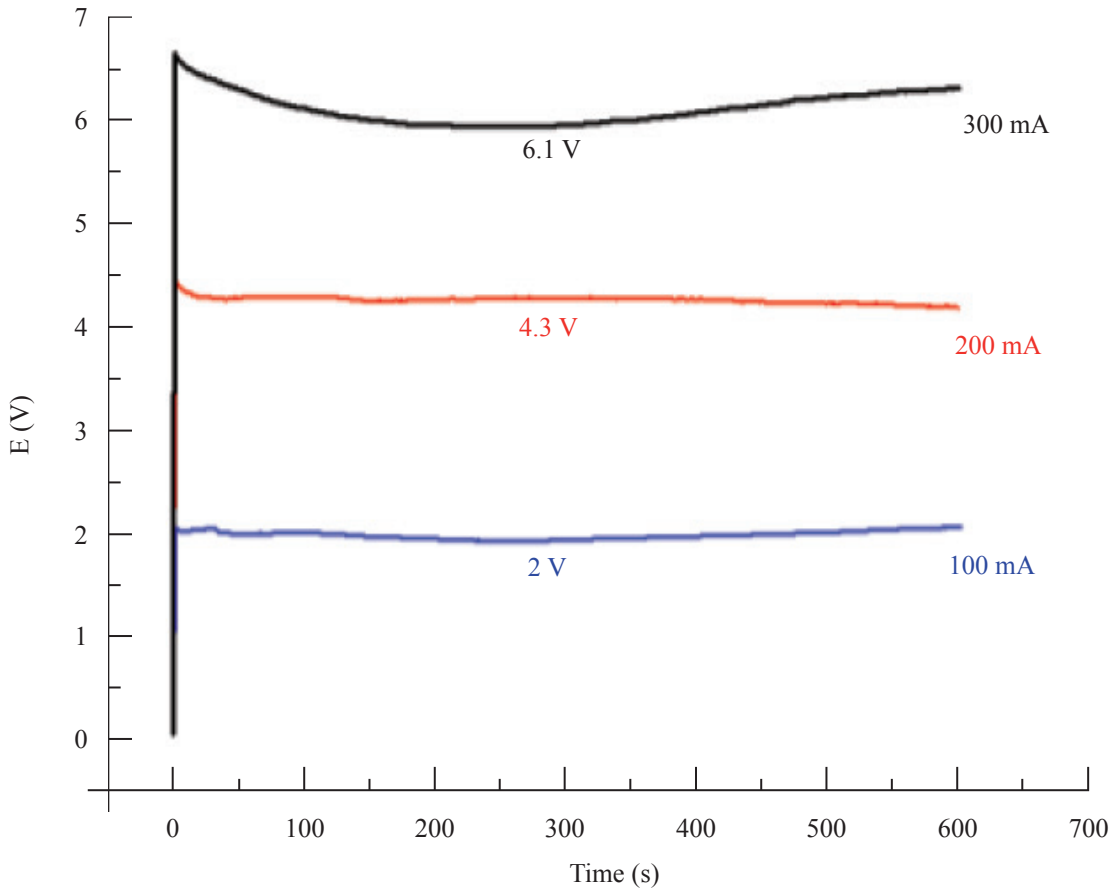

Figure 1. The variation of potential according to time of CuBTC synthesis process at different current intensity.

increased leading to the responding potential increase; the synthesis process happened faster and the mass of CuBTC increased.

The IR spectra of CuBTC synthesized at different applied current intensity (100 mA, 200 mA and 300 mA) are shown in Figure 2. In general, the IR spectra of the samples which were synthesized at different applied currents intensity had the same shape. The peaks appeared in the range 1391 – 1628 cm^{-1} which characterized the COO- group of CuBTC; the peaks at about 1232 cm^{-1} related to the bending mode of -OH group of acid [26, 27] was not observed.

Figure 3 presents X-ray diffraction pattern of CuBTC synthesized at the different applied current intensity. Compared with the published results of others, we could see that synthesized CuBTC had a 3D structure corresponding with the formula $Cu_3(BTC)_2$ expressed in 2 θ value in Table 2. The peak corresponding with the crystal plane which had the Miller index (222) was the highest intensity (Table 2). The phase structure of CuBTC was not affected by the change of applied current in the range from 100 to 300 mA.

From the X-ray diffraction pattern, we could determine the crystal lattice parameter *a* (Table 2) of CuBTC 3D following the equation (*). The crystal lattice parameter *a* changed from 26.44 to 26.46 Å, corresponds with the findings of other researchers [28].

Table 3 shows the product mass obtained in the solution of the samples which were synthesized

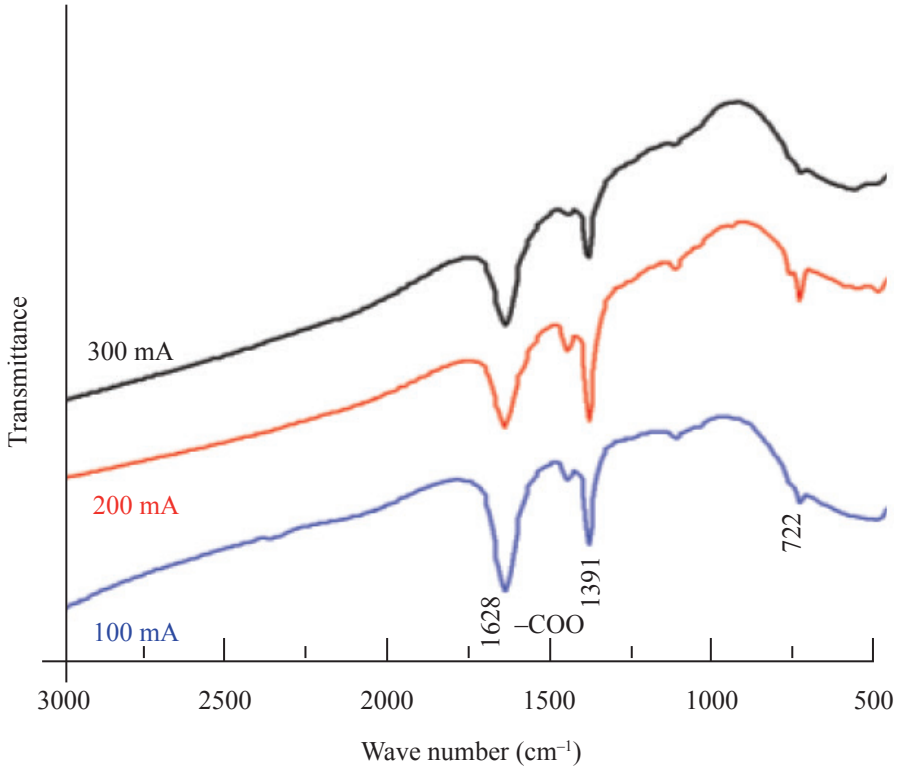

Figure 2. IR spectra of CuBTC synthesized at 100, 200 and 300 mA of different current intensity.

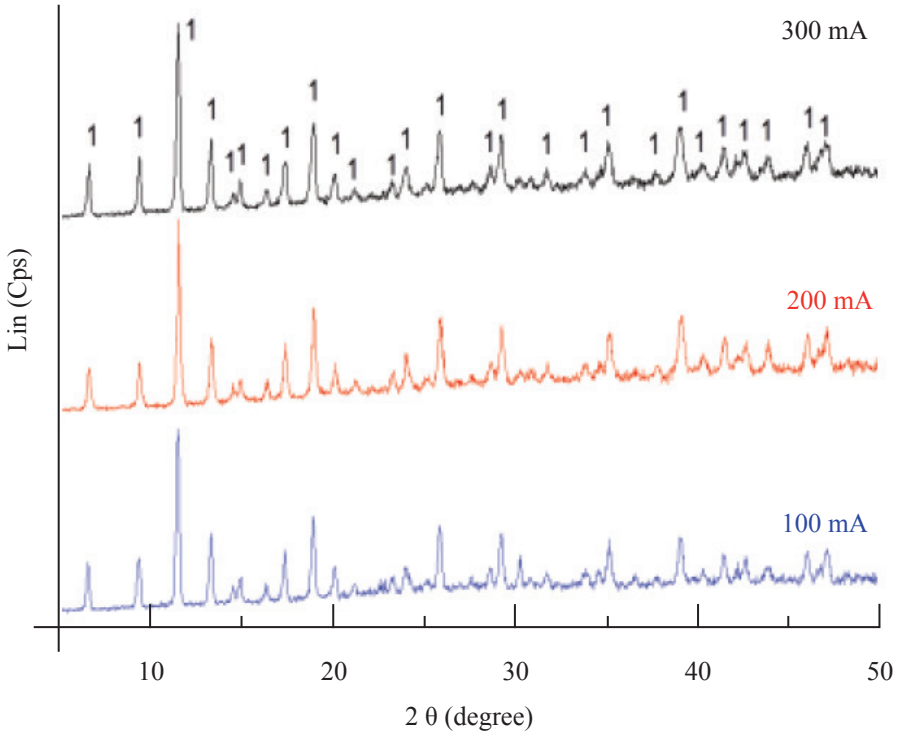

Figure 3. X-ray diffraction pattern of Cu-BTC synthesized at 100, 200 and 300 mA current intensity (1-CuBTC 3D).

Table 2. 2θ value, (hkl) plane, distance between the crystal planes *d* and lattice parameter *a* of CuBTC synthesized at the different current intensity.

(hkl)	2θ [29]	2θ Cu-BTC			*d* (Å)			*a* (Å)		
		M1	M2	M3	M1	M2	M3	M1	M2	M3
200	6.67	6.61	6.64	6.96	13.34	13.25	13.30	26.68	26.50	26.50
220	9.45	9.3	9.37	10.25	9.39	9.36	9.39	26.58	26.50	26.58
222	11.6	11.56	11.65	11.49	7.65	7.64	7.65	26.51	26.49	25.52
400	13.4	13.38	13.27	13.26	6.62	6.62	6.62	26.48	26.50	26.50
331	14.61	14.53	14.54	14.46	6.08	6.06	6.07	26.52	26.44	26.49
420	14.98	14.87	14.97	14.89	5.92	5.92	5.93	26.51	26.52	26.52
422	16.43	16.29	16.34	16.43	5.41	5.41	5.41	26.50	26.50	26.53
511	17.46	17.43	17.44	17.36	5.10	5.10	5.09	26.51	26.50	26.50
440	19.02	18.88	18.88	18.88	4.68	4.68	4.86	26.49	26.47	27.49
600	20.16	20.04	20.17	20.09	4.41	4.41	4.41	26.47	26.47	26.48
620	21.27	21.18	21.12	21.27	4.18	4.18	4.18	26.49	26.49	26.46
444	23.33	23.33	23.32	23.24	3.81	3.82	3.82	26.44	26.49	26.45
551	24.07	24.02	–	24.08	3.70	3.70	3.70	26.45	26.46	26.44
640	24.31	–	–	24.93	–	–	–	–	–	–
642	24.23	–	–	–	3.53	3.53	3.53	26.45	26.47	26.47
731	25.91	25.84	25.94	25.94	3.44	3.44	3.44	26.44	26.46	26.45
733	27.65	27.46	27.57	27.57	3.23	3.23	3.23	26.45	26.46	26.46
660	28.68	28.60	28.58	28.59	3.11	3.11	3.11	26.43	26.43	26.45
751	29.29	29.21	29.17	29.26	3.05	3.05	3.05	26.43	26.47	26.46
840	30.29	30.29	30.19	30.19	2.95	2.95	2.95	26.40	26.47	26.43
911	30.85	–	30.88	30.89	2.89	2.90	2.90	26.40	26.43	26.44
664	31.78	31.74	31.65	31.82	2.82	2.82	2.82	26.44	26.45	26.45
860	33.95	33.74	33.76	33.77	2.64	2.65	2.65	26.48	26.51	26.52
1020	34.64	34.73		34.63	2.59	–	2.59	26.44	–	26.43
951	35.18	35.19	35.05	35.05	2.55	2.55	2.55	26.42	26.45	26.44
1111	37.77	37.86	37.59	37.69	2.38	2.38	2.38	26.44	26.45	26.43
971	39.08	39.16	38.96	39.13	2.31	2.31	2.31	26.39	26.42	26.42
973	40.28	40.25	40.15	40.15	2.24	2.24	2.24	26.41	26.41	26.43
1151	41.50	41.39	41.33	41.51	2.17	2.18	2.18	26.42	26.43	26.43
1222	42.21	42.53	42.11	42.62	2.14	2.14	2.14	26.43	26.45	26.43
1153	42.67	–	42.62	–	2.12	2.12	2.12	26.42	26.44	26.43
1080	43.92	43.84	43.72	43.81	2.06	2.06	2.06	26.44	26.44	26.46
1082	44.48	44.53	44.65	–	–	–	–	–	–	–
1331	45.99	45.90	45.85	45.94	1.97	1.97	1.97	26.41	26.42	26.41
1333	47.11	47.20	46.95	47.04	–	1.932	–	–	26.42	–
a average								26.46	26.46	26.44

at the different applied current intensity. When the applied current intensity increased, the mass of product also increased. However, with the experiments performed at 200 mA and 300 mA, on the electrode surface we could see some black products. It was due to the oxidation of copper metal to copper oxide Cu_2O, the black product might flow down to the solution, mix with the CuBTC powder, leading to a decrease in the purity of product. Therefore, the 100 mA applied current intensity was suitable to synthesize CuBTC.

Table 3. The mass of CuBTC synthesized at the different applied current intensity.

Current intensity (mA)	100	200	300
Mass of CuBTC (g)	0.05619	0.07586	0.16511

The Effect of the $NaNO_3$ Conductor Concentration

The solution to synthesize CuBTC had small conductivity, so we had to add the conductor to increase the conductivity ability of the synthesis solution. In this part, we investigated the influence of $NaNO_3$ conductor concentration to CuBTC synthesis process with 0.05M H_3BTC. When the concentration of $NaNO_3$ changed to 0.05 M, 0.1 M and 0.2 M, the variation of the respond potential following the synthesis time is shown in Figure 4. Three synthesis curves had the same shapes. At the beginning, the potential increases were fast corresponding to the formation of the double layers of BTC ions on the electrode surface, after that the potential had a stable value corresponding with the synthesis process. When the concentration of $NaNO_3$ increased, the potential decreased. This could be explained as: when the $NaNO_3$ concentration was increased, the conductivity of solution increased; the Ohms voltage drop of the solution decreased, leading to a responding potential decrease. The stable potential values obtained at 0.7; 1.1 and 1.26 V/SCE corresponding to $NaNO_3$ concentration were 0.2; 0.1 and 0.05 M.

IR spectra of CuBTC synthesized with the different conductor concentration had the same shape (Figure 6). The peaks in the range 1380 – 1640 cm^{-1} were characteristic of the molecular vibration of –COO group. We also could observe the peak at 1237 cm^{-1} (for H_3BTC at 1273 cm^{-1} in Figure 5) characteristic of the vibration of bending mode of –OH group of acid for the samples have $NaNO_3$ concentration of 0.1 M and 0.2 M [26, 27]. Therefore, in the synthesis solution containing 0.05 M $NaNO_3$, H_3BTC acid was protonated fully. With the $NaNO_3$ concentration of 0.1 M and 0.2 M, acid H_3BTC was only protonated partly.

The X-ray diffraction patterns of CuBTC synthesized with different concentration of $NaNO_3$ are shown in Figure 7. CuBTC synthesized in the solution containing 0.05 M $NaNO_3$ had 3D structure with characteristic peaks with $2\theta = 6.7°$, 9.5°, 11.6° and 13.5°. When the concentration increased to 0.1 M and 0.2 M, CuBTC had both 3D and 1D structures (Table 4). Having the sample in the solution with a concentration of 0.2 M (saturate concentration), the peak corresponding with CuBTC 1D had higher intensity than CuBTC 3D. CuBTC 1D is called catena-triaqua-μ-[1,3,5-benzentricacboxylato]-copper (II) corresponding to the formula $Cu(BTC)(H_2O)_3$ with characteristic peak values of 2θ: 9.2°, 9.9°, 10.9° and 13.5°. To react with Cu^{2+} ions, the –COOH groups in H_3BTC were protonated, if the protonation was full with three –COOH groups, CuBTC 3D structure would be obtained. In this case only two in three –COOH groups were protonated, CuBTC would have a zigzag structure (1D), the crystals growth followed one direction. CuBTC 3D corresponding to the formula $Cu_3(BTC)_2$ with the characteristic 2θ values 6.7°, 9.5°, 11.6° and 13.5° in which the peak at 11.6° corresponding crystal plane with Miller index (222) had the highest intensity. This result was suitable with the IR spectra above when the characteristic peaks of –OH group of acid were observed with the samples which had $NaNO_3$ concentrations of 0.1 M and 0.2 M. This result could be explained as follow: The use of a higher concentration of the conductive salt in the synthesis resulted in agglomeration and collapse of the cubic crystals shape of the MOF. Conceivably, the MOF material following its formation might have suffered electrolytic degradation in the increasingly conductive medium.

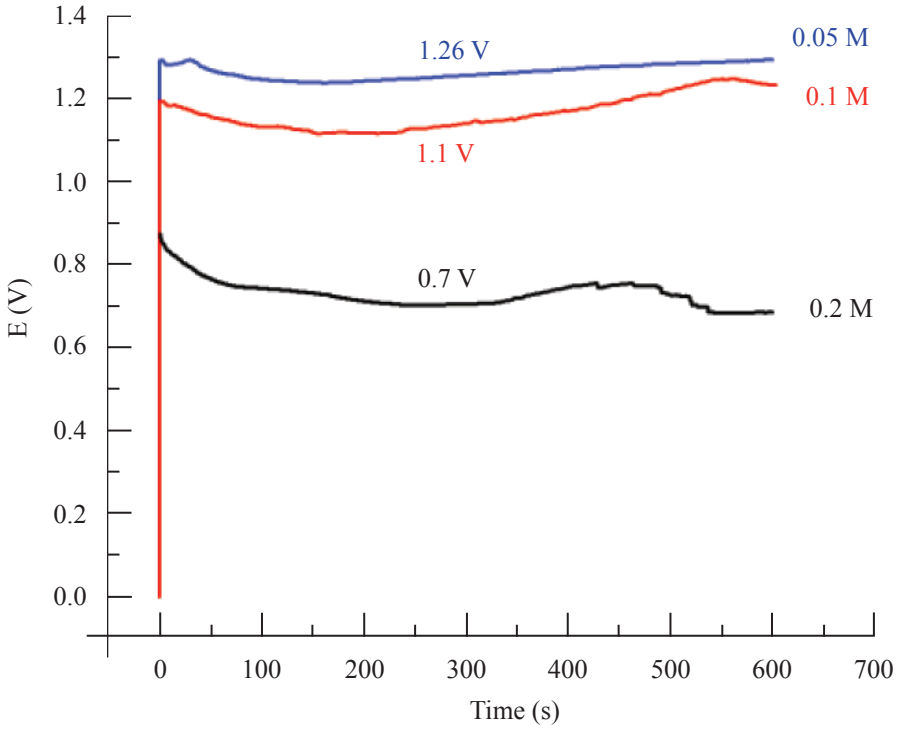

Figure 4. Curve E = f (t) of synthesis process CuBTC at I = 100 mA in solution containing $NaNO_3$ with different concentration.

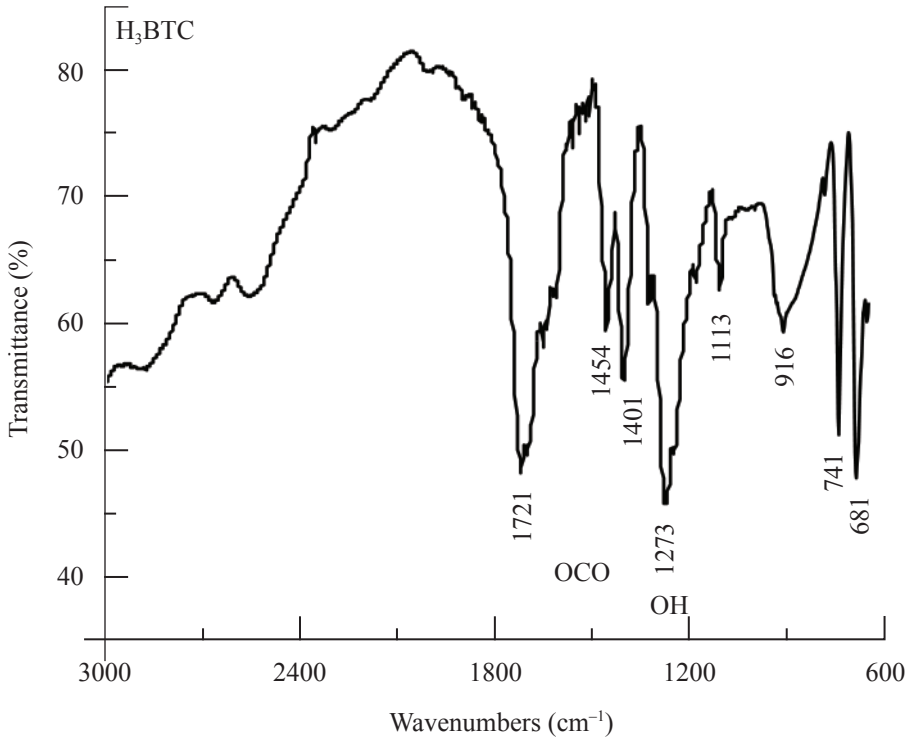

Figure 5. IR spectra of H_3BTC.

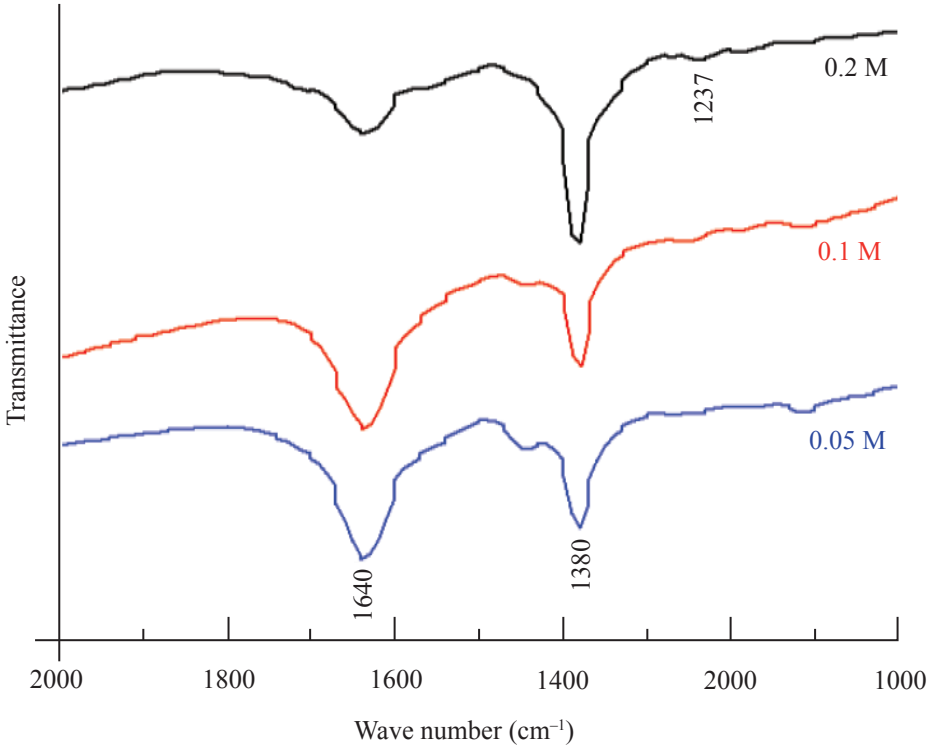

Figure 6. IR spectra of CuBTC synthesized with $NaNO_3$ conductor salt with different concentration in the range of wave number 1000–2000 cm^{-1}.

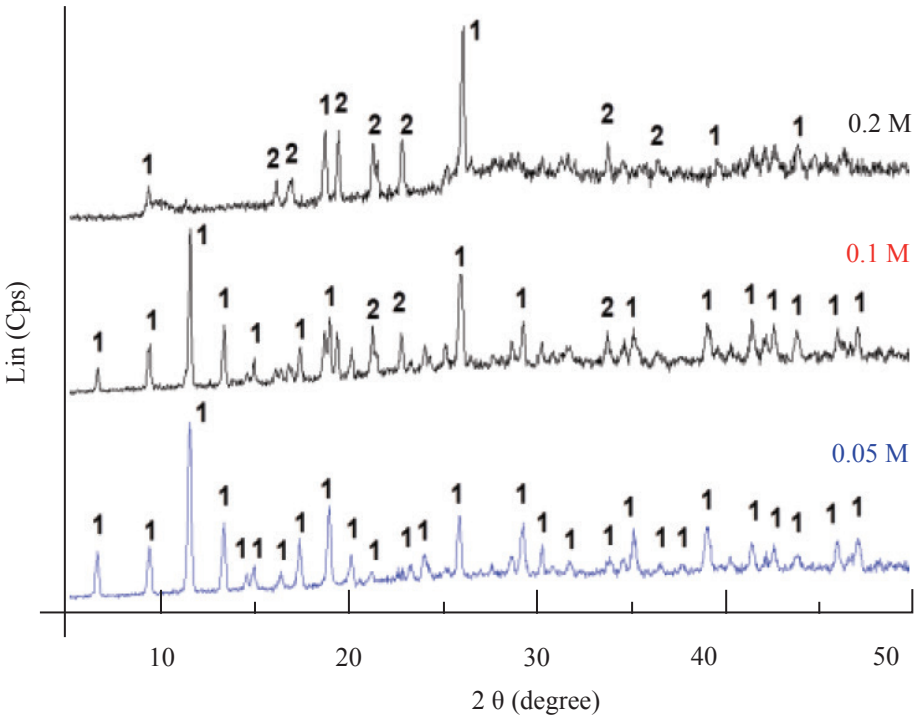

Figure 7. X-ray diffraction pattern of CuBTC synthesized in $NaNO_3$ with different concentration (1- CuBTC 3D and 2- CuBTC 1D).

Table 4. The position of diffraction peaks of CuBTC 1D synthesized with 0.2 M $NaNO_3$ compared with the CuBTC 1D following the literature.

2θ CuBTC 1D [29]	9.3	10	11	13.4	17.1	18.65	21.35	22.2	24.5
2θ (M5)	9.2	–	11	13.5	–	18.6	21.36	22.7	24.35

Table 5. 2θ value, (hkl) plane, the distance between crystal plane *d* and lattice parameter (*a*) of CuBTC synthesized in solution with different $NaNO_3$ conductor concentrations 0.05 M and 0.1 M.

(hkl)	2θ [29]	2θ Cu-BTC synthesis		d (Å)		A (Å)	
		0.05M	0.1M	0.05M	0.1M	0.05M	0.1M
200	6.67	6.61	6.62	13.34	13.22	26.68	26.44
220	9.45	9.3	9.46	9.39	9.39	26.58	26.58
222	11.60	11.56	11.6	7.65	7.64	26.51	26.48
400	13.40	13.38	13.3	6.62	6.61	26.48	26.45
331	14.61	14.53	–	6.08	6.06	26.52	26.42
420	14.98	14.87	14.82	5.92	5.91	26.51	26.43
422	16.43	16.29	–	5.41	5.44	26.50	26.65
511	17.46	17.43	17.40	5.10	5.09	26.51	26.47
440	19.02	18.88	19.04	4.68	–	26.49	–
600	20.16	20.04	20.16	4.41	4.40	26.47	26.424
620	21.27	21.18	21.18	4.18	4.17	26.49	26.39
444	23.33	23.33	23.75	3.81	3.82	26.44	26.44
551	24.07	24.02	24.04	3.70	3.70	26.45	26.43
640	24.31	–	–	–	–	–	–
642	24.23	–	–	3.53	3.54	26.45	26.49
731	25.91	25.84	25.93	3.44	3.43	26.44	26.36
733	27.65	27.46	–	3.23	3.22	26.45	26.37
660	28.68	28.60	–	3.11	3.11	26.43	26.41
751	29.29	29.21	29.47	3.05	3.05	26.43	26.41
840	30.29	30.29	30.24	2.95	2.95	26.40	26.42
911	30.85	–	–	2.89	2.89	26.40	26.40
664	31.78	31.74	31.53	2.82	2.82	26.44	26.47
860	33.95	33.74	33.78	2.65	2.65	26.48	26.54
1020	34.64	34.73	–	2.59	2.59	26.44	26.41
951	35.18	35.19	35.16	2.55	2.55	26.42	26.39
1111	37.77	37.86	–	2.38	–	26.44	–
971	39.08	39.16	39.04	2.30	2.30	26.39	26.37
973	40.28	40.25	–	2.24	2.23	26.41	26.38
1151	41.50	41.39	41.45	2.17	2.17	26.42	26.42
1222	42.21	42.53	–	2.14	2.14	26.43	26.45
1153	42.67	–	42.65	2.12	2.12	26.42	26.41
1080	43.92	43.84	43.78	2.06	2.06	26.44	26.46
1082	44.48	44.53	–	–	–	–	–
1331	45.99	45.90	–	1.97	–	26.41	–
1333	47.11	47.20	47.15	–	1.93	–	26.41
a average						26.46	26.44

From the X-ray diffraction patterns, we could determine the lattice parameter (*a*) of CuBTC 3D following the equation (*). The lattice parameter (*a*) varied from 26.44 to 26.46 Å (Table 5), concurring with lattice parameter (*a*) of CuBTC 3D of other researchers.

When the conductor concentration increased, we could see the colour of solution becoming more dark blue (the amount of product was synthesized more). However, in observing the electrode surface also in the bottom of the cell, its appearance was a black product which was the by-product of the synthesis process. The amount of black product increased when the conductor concentration increased. Therefore, we chose $NaNO_3$ conductor concentration of 0.05M for the next research work.

The Effect of Synthesis Time

Figure 8 presents the variation of potential follow time of CuBTC synthesis process with the 0.05 M $NaNO_3$ conductor in different synthesis time: 10, 20 and 40 min. In general, the synthesis curves had the same shape, at the beginning, the potential increase was fast due to the formation of the double layer of BTC ions on the electrode surface, subsequently, the potential stability was in the range of 1.8 to 2.2 V/SCE.

Figure 9 shows the IR spectra of CuBTC synthesized in the different time with the same shape. The peaks in the range 1383 cm^{-1} to 1632 cm^{-1} was characterics of an –COO group. With the samples synthesized in 20 min and 40 min, we could observe the peaks at 1707 cm^{-1} and 1195 cm^{-1} corresponding with the vibration of C=O and C-O groups.

The X-ray diffraction pattern of CuBTC synthesized with different time was shown in Figure 10. The results showed that CuBTC had 3D structures and were not affected by synthesis time (the characteristic peaks could be observed in Table 6). The lattice parameter *a* (Table 6) of CuBTC 3D was determined by equation (*) varied in the range 26.44 to 26.5 Å which concurred with the lattice parameter of CuBTC 3D of other researchers.

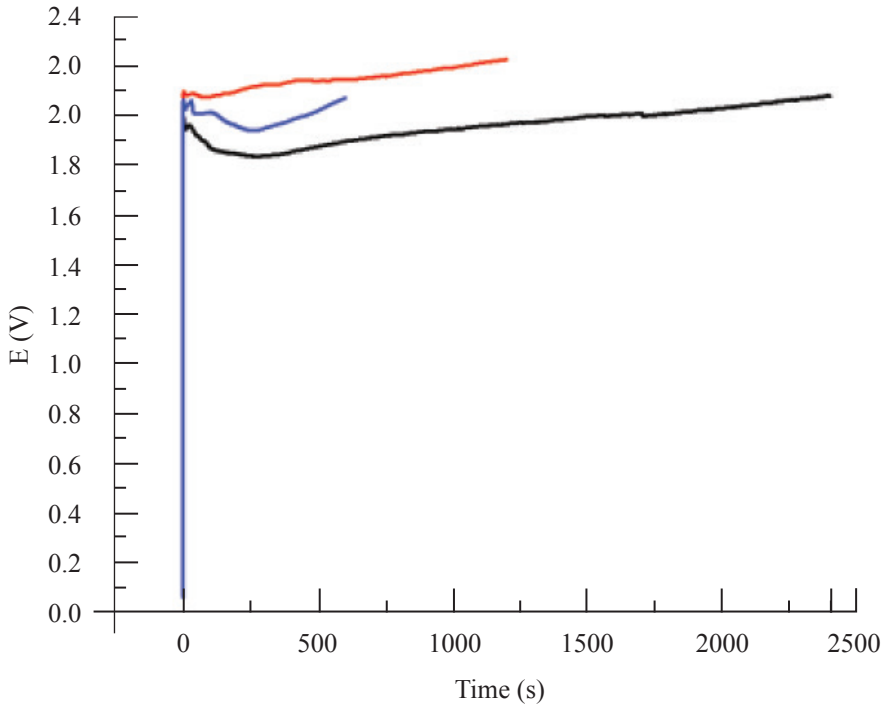

Figure 8. Curve E = f(t) of CuBTC synthesis process at I = 100 mA, 0.05 M $NaNO_3$ with different synthesis time.

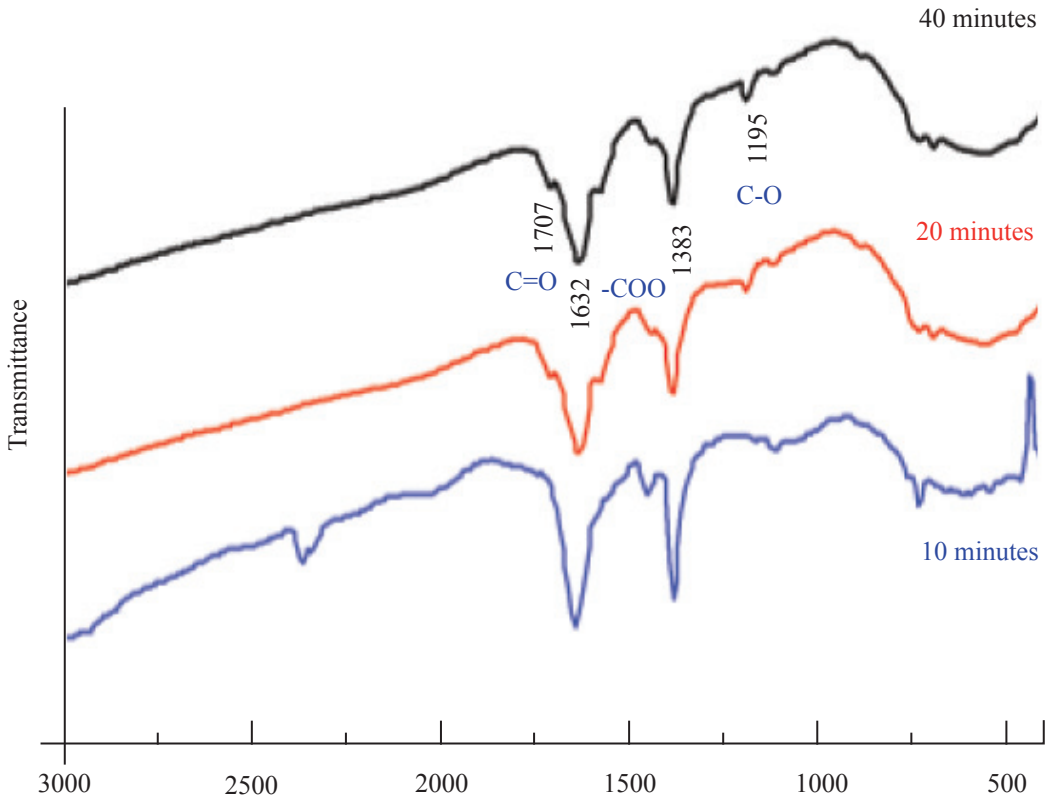

Figure 9. IR spectra of CuBTC synthesized with different time.

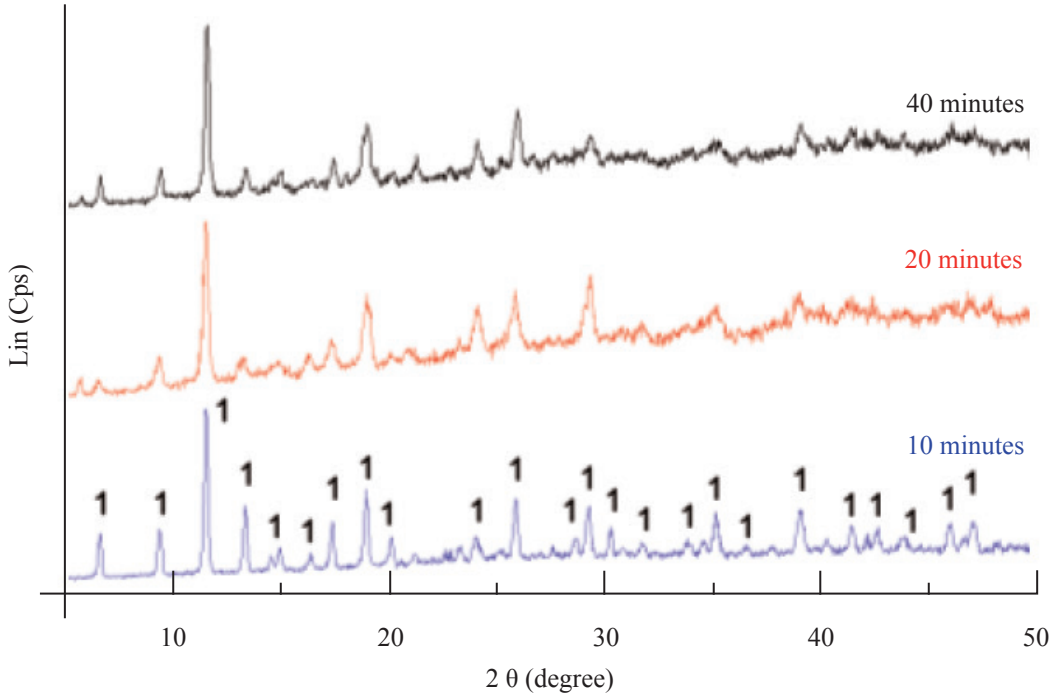

Figure 10. X-ray diffraction pattern of CuBTC synthesized in $NaNO_3$ with different synthesis time.

Table 6. 2θ value, (hkl) plane, the distance between the crystal plane *d* and crystal lattice parameter *a* of CuBTC synthesized with different time: 10, 20 and 40 min.

(hkl)	2θ [29]	2θ Cu-BTC			d (Å)			a (Å)		
		M1	M4	M5	M1	M4	M5	M1	M4	M5
	5.73	–	5.76	5.72	–	15.45	15.25	–	26.76	26.41
200	6.68	6.61	6.52	6.68	13.34	13.44	13.26	26.68	26.88	26.52
220	9.46	9.3	9.3	9.43	9.39	9.43	9.38	26.58	26.68	26.53
222	11.60	11.56	11.54	11.58	7.65	7.66	7.63	26.51	26.55	26.41
400	13.40	13.38	13.34	13.37	6.62	6.67	6.61	26.48	26.67	26.44
331	14.62	14.53	–	–	6.08	–	–	26.52	–	–
420	14.99	14.87	14.87	14.99	5.92	5.92	5.91	26.51	26.62	26.42
422	16.44	16.29	16.33	–	5.41	5.43	–	26.50	26.62	–
511	17.46	17.43	17.37	17.44	5.10	5.11	5.08	26.51	26.54	26.42
440	19.02	18.88	19.51	–	4.68	4.67	–	26.49	26.41	–
600	20.17	20.04	20.93	–	4.41	4.22	–	26.47	26.67	–
620	21.27	21.18	–	21.31	4.19	–	4.18	26.49	–	26.42
444	23.33	23.33	23.27	–	3.82	3.69	–	26.44	25.59	–
551	24.07	24.02	24.15	24.10	3.70	–	3.69	26.45	–	26.37
640	24.32	–	–	–	–	–	–	–	–	–
642	24.24	–	–	–	3.53	–	–	26.45	–	–
731	25.91	25.84	25.80	25.94	3.44	3.44	3.53	26.44	26.48	26.40
733	27.65	27.46	–	27.62	3.23	–	–	26.45	–	–
660	28.68	28.60	–	–	3.12	–	–	26.43	–	–
751	29.29	29.21	29.30	29.30	3.05	3.04	3.05	26.43	26.39	26.37
840	30.29	30.29	–	–	2.95	–	–	26.40	–	–
911	30.86	–	–	–	2.89	–	–	26.40	–	–
664	31.78	31.74	31.74	–	2.82	2.81	–	26.40	26.44	–
860	33.95	33.74	–	–	2.64	–	–	26.48	–	–
1020	34.64	34.73	–	–	2.59	–	–	26.44	–	–
951	35.18	35.19	35.19	35.05	2.55	2.55	–	26.42	26.45	–
1111	37.77	37.86	–	–	2.38	–	–	26.44	–	–
971	39.08	39.16	39.02	39.12	2.30	2.31	2.30	26.39	26.43	26.39
973	40.28	40.25	–	–	2.24	–		26.41	–	–
1151	41.50	41.39	41.41	41.41	2.18	–	2.18	26.42	–	26.42
1222	42.21	42.53	42.37	–	2.14	–		26.43	–	–
1153	42.67	–	–	42.66	2.12	–	2.12	26.42	–	26.15
1080	43,.92	43.84	–	43.80	2.06	2.06	2.06	26.44	26.44	26.47
1082	44.48	44.53	–	–	–	–	–	–	–	–
1331	45.99	45.90	–	–	1.97	2.00	–	26.41	26.79	–
1333	47.11	47.20	47.83	47.83	–	1.93	–	–	26.45	–
			a average					26.46	26.5	26.44

Table 7. The mass of CuBTC synthesized with 10, 20 and 40 min.

Synthesis time (min)	Mass of product (g)
10	0.05619
20	0.07210
40	0.10960

Synthesis time increased leading to the mass of product increase which was shown in Table 7, however, in synthesis process, when the synthesis time increased, the amount of black product (could be Cu_2O) on the surface of electrode and the bottom of cell also increased. This switching of the redox state in solution could perhaps be aided by the formation of chloro-complexes with the Cl^- ions coming from leakage of the calomel electrode [30]. From the experiment, we chose the most suitable synthesis time of 10 min.

Figure 11 presents SEM images of the sample synthesized in the optimum condition: concentration of H_3BTC and $NaNO_3$ were 0.05 M in 10 min with the applied current intensity of 100 mA. CuBTC had a block shape, large sized in the range of 100 nm to 1.2 μm.

The Influence of Hydrate Process

CuBTC 3D sample synthesized in the optimum condition: the concentration of H_3BTC and $NaNO_3$ was 0.05M in 10 min with applied current intensity 100 mA, filtered and rinsed by methanol. Subsequently a part was dried at 60°C and another a part was immersed in water for 5 min, 4 h, then the sample was vacuumed, dried at 60°C, under 250 mBar pressure for 15 h. We could observe the phenomenon of CuBTC expand after immersion in water, it could be called breath effect of metal organic framework. The hydrate process might increase the specific surface area and also the size and the pore volume of CuBTC, but it could lead to the reaction of water with opening metal centers and change the phase structure of CuBTC with a large enough hydrate time. From the X-ray diffraction pattern of CuBTC samples which was immersed in water (Figure 12), we could see the hydrate process affected by the phase structure of CuBTC. The CuBTC sample after filtering, rinsing, dried at 60°C, or immersed in water for a short time (5 min) still kept the 3D phase structure with the characteristic 2 θ value. However, when hydrate product immersed in water for 4 h, the phase structure of CuBTC was changed [31]. In the X-ray diffraction pattern, the characteristic peaks of CuBTC 3D were not observed. Instead of that, the 2 θ values are 7.81°; 9.07°; 11.36°; 12.03° corresponding with other chemicals of copper $C_8H_4CuO_4.3H_2O$, C_6H_5Cu, $C_4H_4CuO_4.2H_20$.

To confirm the effect of hydrate process to specific surface area of sample, the CuBTC 3D powder synthesized with applied current intensity 100 mA with the synthesis time of 10 min, immersed in water with different times: 0 min, 5 min and 4 h, after which the specific surface area of sample was

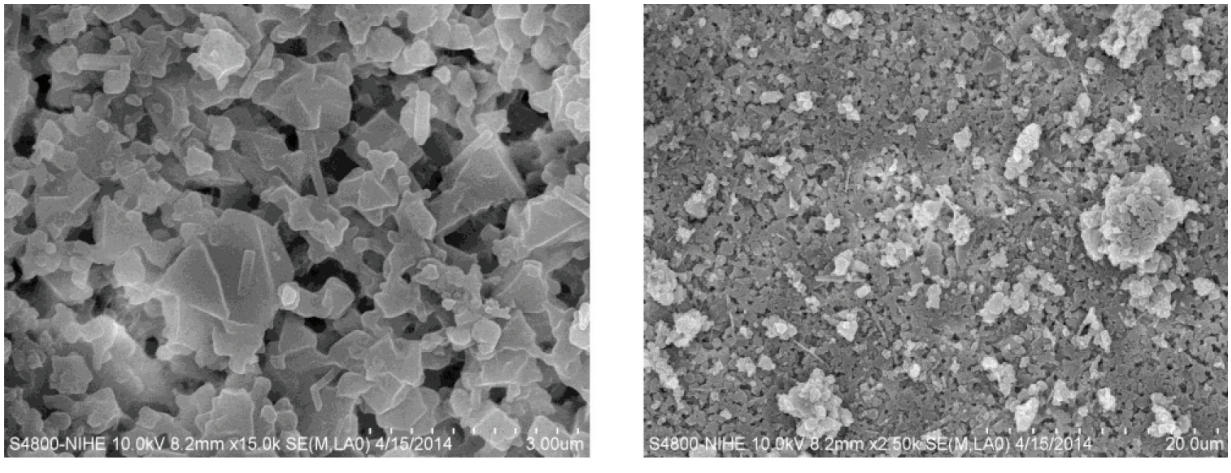

Figure 11. SEM image of CuBTC 3D synthesized in the optimum condition.

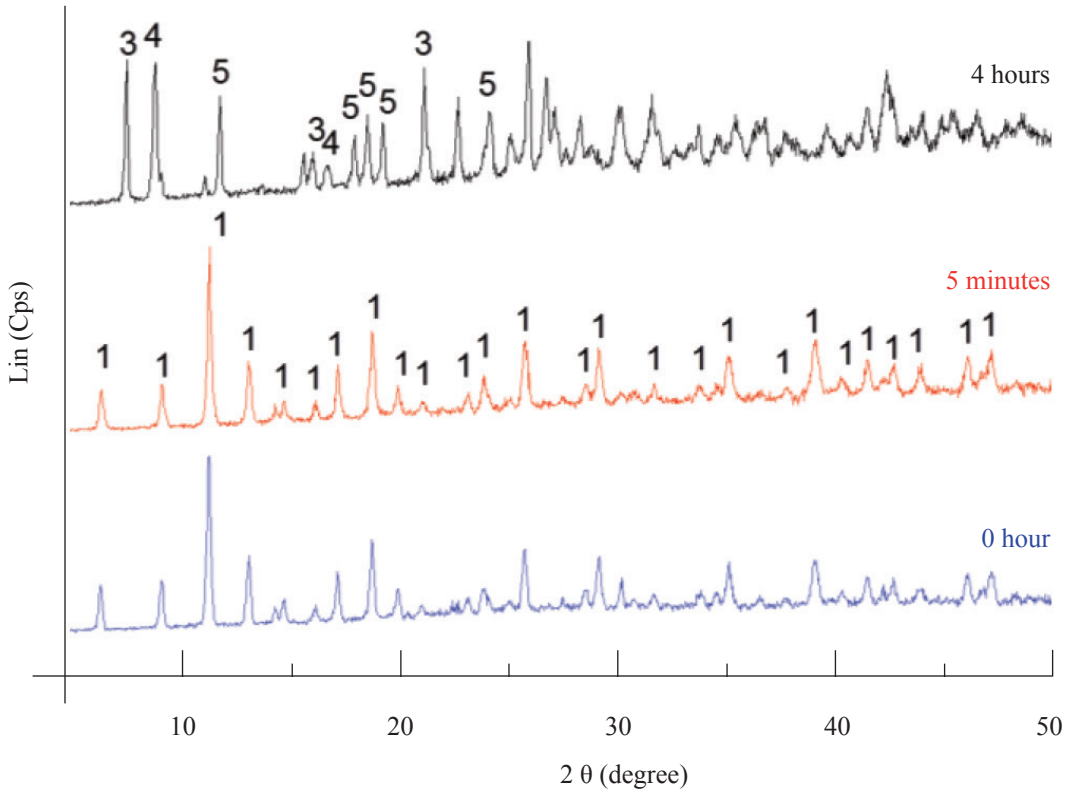

Figure 12. The Xray diffraction pattern of CuBTC hydrated: 0 min, 5 min and 4 h (1-CuBTC-3D, 3- $C_8H_4CuO_4.3H_2O$; 4-C_6H_5Cu; 5-$C_4H_4CuO_4.2H_2O$).

determined by N_2 absorption. Figure 13 presents the N_2 absorption isotherm curves of CuBTC powder which hydrated with different time. There was hysteresis with de-absorption, so that we could predict that the material is mesoporous.

The specific surface area was determined from BET curve (Figure 14) in the relative pressure from 0.05 to 0.23. CuBTC 3D hydrate in 5 min, 617 m^2/g specific surface area increased about 7.8 times compared with CuBTC without hydration treatment (79 m^2/g). With the sample CuBTC 3D hydrated in 4 h, the specific surface area was only 2.7 m^2/g. The short-time hydrate did not only change the phase structure of CuBTC but also increased the specific surface area and the pore volume of material (Table 8). However, the long-time hydrate process could destroy the structure of CuBTC 3D leading to a decrease in the specific surface area.

Table 8. The specific surface area, pore diameter and pore volume of the samples which were hydrated at different time.

Hydrated time	0 hour	5 minutes	4 hours
Specific surface area (m^2/g)	79	617	2.8
Pore diameter (nm)	5.3	2.4	17.2
Pore volume (cm^3/g)	0.104678	0.376909	0.011896

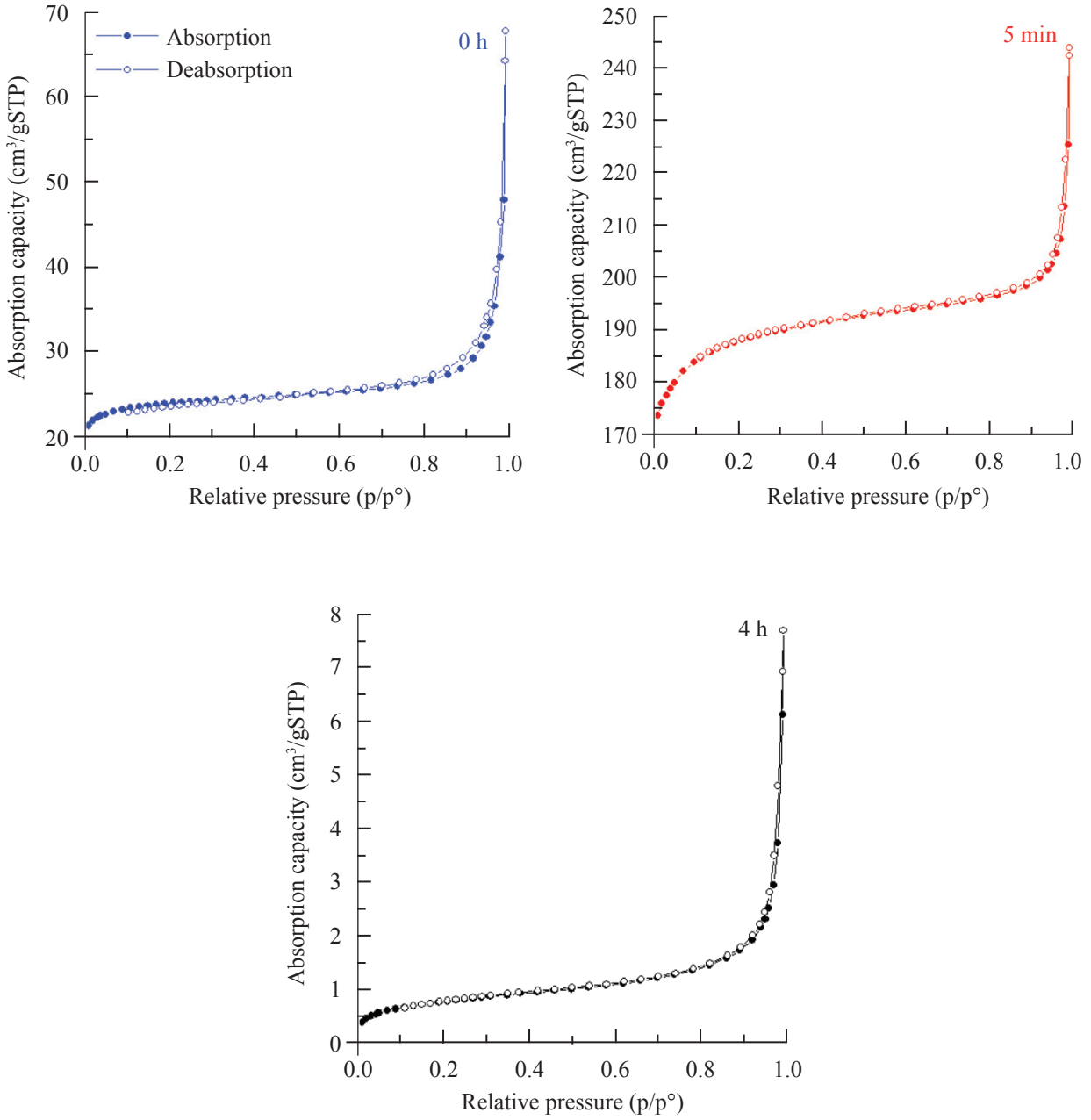

Figure 13. The BET absorption isothermal curve of CuBTC which was hydrated at different time: 0 h, 5 min and 4 h.

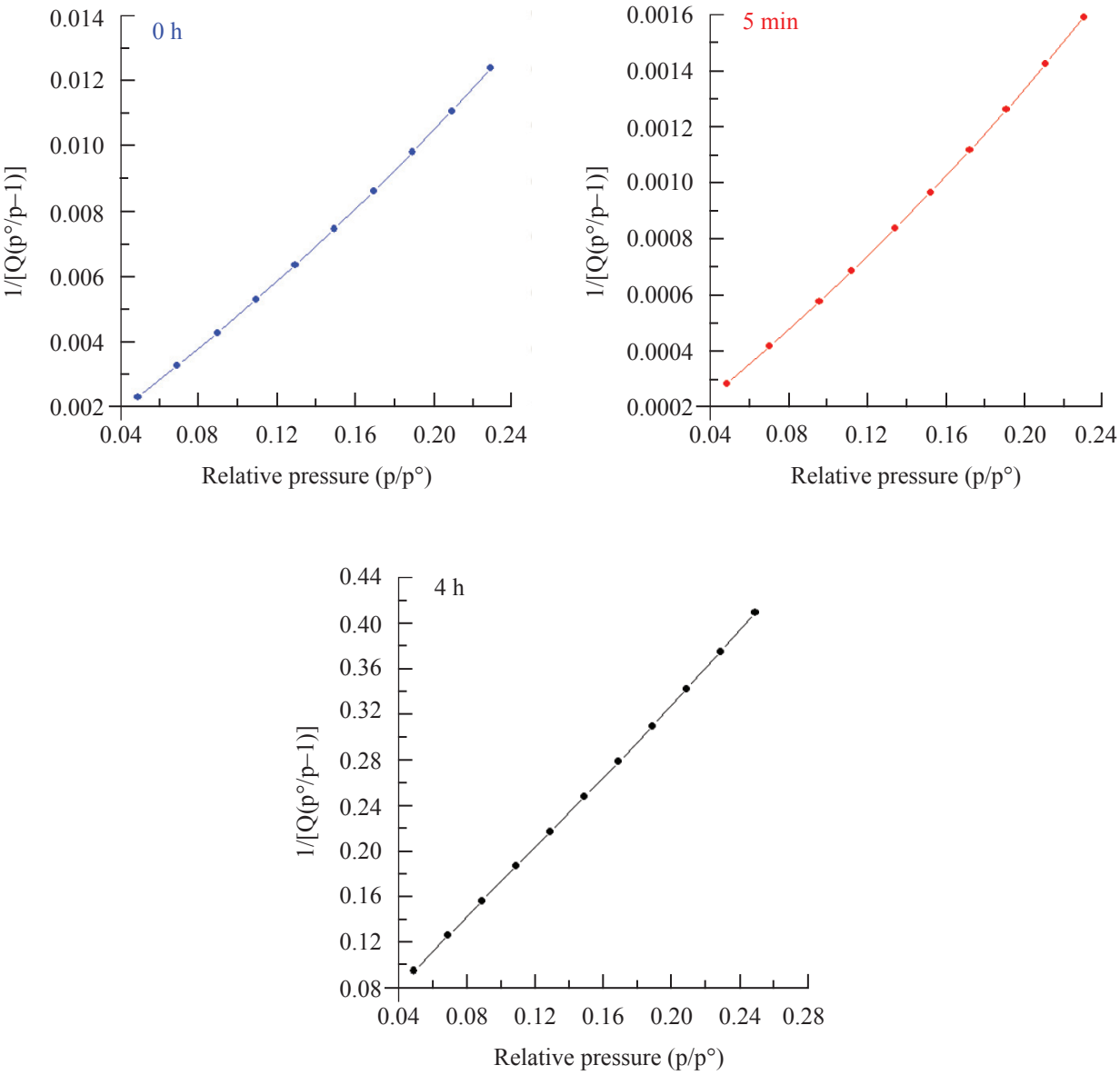

Figure 14. BET curves of CuBTC synthesized with different hydrated time: 0 h, 5 min and 4 h.

CONCLUSION

CuBTC was successfully synthesized by applied current method. Depending on the synthesis conditions, we obtained CuBTC 1D or 3D structures, but CuBTC was obtained with a small specific surface area due to the breath effect. When CuBTC was hydrated by soaking in water for 5 min, the specific surface area increased to 7.8 times however, with the soaking time of 4 h, CuBTC structures were destroyed leading to a decreased specific surface area. Studies to improve the stability and the specific surface area of CuBTC 3D is needed and should be continued in the future.

REFERENCE

1. Yaghi, O.M., Li, G and Li, H. (1995) Selective binding and removal of guests in a microporous metal-organic framework, *Nature*, **378**, 703−706.
2. Chui, S.S.-Y., Lo, S.M.-F., Charmant, J.P.H., Orpen, A.G. and Williams, I.D. (1999) A chemically functionalizable nanoporous material, $[Cu_3(TMA)_2(H_2O)_3]_n$, *Science*, **283**, 1148−1150.
3. Tranchemontagne, D.J., Hunt, J.R. and Yaghi, O.M. (2008) Room temperature synthesis of metal-organic frameworks: MOF-5, MOF-74, MOF-177, MOF-199, and IRMOF-0, *Tetrahedron,* **64,** 8553−8557.
4. Wang, X., Lin, H., Bi, Y., Chen, B. and Liu, G. (2008) An unprecedented extended architecture constructed from a 2-D interpenetrating cationic coordination framework templated by $SiW_{12}O_{40}^{4-}$ anion, *Journal of Solid State Chemistry*, **181**, 556−561.
5. Kayaert, S., Bajpe, S., Masschaele, K., Breynaert, E., Kirschhock, C.E.A. and Martens, J.A. (2011) Direct growth of Keggin polyoxometalates incorporated copper 1,3,5-benzenetricarboxylate metal organic framework films on a copper metal substrate, *Thin Solid Films*, **519**, 5437–5440.
6. Yang, H., Orefuwa, S. and Goudy, A. (2011) Study of mechanochemical synthesis in the formation of the metal–organic framework $Cu_3(BTC)_2$ for hydrogen storage, *Microporous and Mesoporous Materials*, **143**, 37–45.
7. Brown, C.M., Liu, Y. and Neumann, D.A. (2008) Neutron powder diffraction of metal-organic frameworks for hydrogen storage, *Journal of Physics*, **71**, 755–760.
8. Li, Z-Q., Qiu, L-G., Xu, T., Wu, Y., Wu, Y., Wang, W., Wu, Z-Y. and Jiang, X. (2009) Ultrasonic synthesis of the microporous metal-organic framework $Cu_3(BTC)_2$ at ambient temperature and pressure: An efficient and environmentally friendly method, *Materials Letters***, 63**, 78−80.
9. Schlesinger, M., Schulze, S., Hietschold, M. and Mehring, M. (2010) Evaluation of synthetic methods for microporous metal–organic frameworks exemplified by the competitive formation of $[Cu_2(btc)_3(H_2O)_3]$ and $[Cu_2(btc)(OH)(H_2O)]$, *Microporous and Mesoporous Materials* **132**, 121–127.
10. Assche, T.R.C.V. and Denayer, J.F.M. (2013) Fabrication and separation performance evaluation of a metal–organic framework based microseparator device, *Chemical Engineering Science,* **95**, 65–72.
11. Campagnol, N., Assche, T.V., Boudewijns, T., Denayer, J., Binnemans, K., Vos, D.D. and Fransaer, J. (2013) High pressure, high temperature electrochemical synthesis of metal–organic frameworks: films of MIL-100 (Fe) and HKUST-1 in different morphologies, *J. Mater. Chem. A,* **1**, 5827−5830.
12. Kumar, R.S., Kumar, S.S. and Kulandainathan, M.A. (2013) Efficient electrosynthesis of highly active $Cu_3(BTC)_2$-MOF and its catalytic application to chemical reduction, *Microporous and Mesoporous Materials*, **168**, 57–64.
13. Hartmann, M., Kunz, S., Himsl, D., and Tangermann, O. (2008) Adsorptive separation of isobutene and isobutane on $Cu_3(BTC)_2$, *Langmuir,* **24**, 8634−8642.
14. Joaristi, M., Juan-Alcañiz, J., Serra-Crespo, P., Kapteijn, F. and Gascon, J. (2012) Electrochemical synthesis of some archetypical Zn^{2+}, Cu^{2+}, and Al^{3+} metal organic frameworks, *Cryst. Growth Des.,* **12**, 3489−3498.
15. Ameloot, R., Stappers, L., Fransaer, J., Alaerts, L., Sels, B.F. and Vos, D.E.D. (2009) Patterned growth of metal-organic framework coatings by electrochemical synthesis, *Chem. Mater*., **21**, 2580–2582.
16. Kumar, R.S., Kumar, S.S. and. Kulandainathan, M.A. (2012) Highly selective electrochemical reduction of carbon dioxide using Cu based metal organic framework as an electrocatalyst, *Electrochemistry Communications*, **25**, 70–73.
17. Assche, T.R.C.V., Desmet, G., Ameloot, R., Vos, D.E.D., Terryn, H. and Denayer, J.F.M. (2012) Electrochemical synthesis of thin HKUST-1 layers on copper mesh, *Microporous and Mesoporous Materials*, **158**, 209–213.
18. Gascon, J., Aguado, S. and Kapteijn, F. (2008) Manufacture of dense coatings of $Cu_3(BTC)_2$ (HKUST-1) on a-alumina, *Microporous and Mesoporous Materials*, **113**, 132–138.
19. Mueller, U., Schubert, M., Teich, F., Puetter, H., Schierle-Arndt K. and Pastre´, J. (2006) Metal–organic frameworks—prospective industrial applications, *J. Mater. Chem*., 16, 626–636.
20. Yang, H.M., Song, X.L., Yang, T.L., Liang, Z.H. and Hao, X.G. (2014) Electrochemical synthesis of flower shaped morphology MOFs in an ionic

liquid system and their electrocatalytic application to the hydrogen evolution reaction, *RSC Adv.,* **4**, 15720–15726.

21. Hartmann, M., Himsl, D., Kunz, S. and Tangermann, O. (2008) Olefin/paraffin separation over the metal organic framework material $Cu_3(BTC)_2$, *Zeolites and Related Materials*, **174**, Part **A**, 615–618.
22. Rowsell, J.L.C. and Yaghi, O.M. (2005) Strategies for hydrogen storage in metal–organic frameworks, *Angew. Chem. Int. Ed.,* **44**, 4670–4679.
23. Rowsell, J.L.C. and Yaghi, O.M. (2006) Effects of functionalization, catenation, and variation of the metal oxide and organic linking units on the low-pressure hydrogen adsorption properties of metal-organic frameworks, *J. Am. Chem. Soc.,* **128 (4)**, 1307–1315.
24. Llabrés i Xamena, F.X., Abad, A., Corma, A. and Garcia, H. (2007) MOFs as catalysts: Activity, reusability and shape-selectivity of a Pd-containing MOF, *Journal of Catalysis,* **250**, 294–298.
25. Opelt, S., Türk, S., Dietzsch, E., Henschel, A., Kaskel, S. and Klemm, E. (2008) Preparation of palladium supported on MOF-5 and its use as hydrogenation catalyst, *Catalysis Communications*, **9(6)**, 1286–1290.
26. Marx, S., Kleist, W. and Baiker, A. (2011) Synthesis, structural properties, and catalytic behavior of Cu-BTC and mixed-linker Cu-BTC-PyDC in the oxidation of benzene derivatives, *Journal of Catalysis,* **281,** 76–87.
27. Seo, Y-K., Hundal, G., Jang, I.T., Hwang, Y.K., Jun, C-H. and Chang, J-S. (2009) Microwave synthesis of hybrid inorganic–organic materials including porous $Cu_3(BTC)_2$ from Cu(II)-trimesate mixture, *Microporous and Mesoporous Materials,* **119,** 331–337.
28. Starosta, W., Sartowska, B., Łyczko, K., Maurin, J., Pawlukojć, A., Waliś, L. and Buczkowski, M. (2012) A method for production of nano MOF and prelimiary characterization by selected analytical techniques, *Nukleonika*, **57(4)**, 581−583.
29. Gascon, J., Aguado, S. and Kapteijn, F. (2008) Manufacture of dense coatings of $Cu_3(BTC)_2$ (HKUST-1) on a-alumina, *Microporous and Mesoporous Materials*, **113,** 132–138.
30. Yin, J., Qi, L. and Wang, H. (2012) Antifreezing Ag/AgCl reference electrodes: Fabrication and applications, *Journal of Electroanalytical Chemistry*, **666**, 25–31.
31. Decoste, J.B., Peterson, G.W., Smith, M.W., Stone, C.A. and Willis, C.R. (2012) Enhanced stability of Cu-BTC MOF via perfluorohexane plasma-enhanced chemical vapor deposition, *Journal of the American Chemical Society,* **134**, 1486–1489.